Tuning phonon properties to enhance the thermoelectric figure of merit

Iorwerth O. Thomas and G. P. Srivastava

Citation: AIP Conference Proceedings **1590**, 95 (2014); doi: 10.1063/1.4870203
View online: http://dx.doi.org/10.1063/1.4870203
View Table of Contents: http://scitation.aip.org/content/aip/proceeding/aipcp/1590?ver=pdfcov
Published by the AIP Publishing

Tuning phonon properties to enhance the thermoelectric figure of merit

Iorwerth O. Thomas and G. P. Srivastava

School of Physics, University of Exeter, Stocker Road, Exeter EX4 4QL, United Kingdom

Abstract.
We will discuss a theory of the thermoelectric properties of semiconductor alloys and superlattices, with an emphasis on the role of phonons. After summarising our previous calculations of the lattice thermal conductivity and the thermoelectric figure of merit ZT of an n-type SiGe alloy system, we will present some recent results for an ultra-thin SiGe superlattice and discuss how they differ from the alloy results.

Keywords: thermoelectric effect, Figure of Merit, superlattices, phonons
PACS: 63.22.-m 63.20.dk 65.40-b

INTRODUCTION

The thermoelectric effect has attracted much theoretical and experimental attention following the discovery that the nanostructuring of semi-conductor compounds can increase their thermoelectric efficiency (as quantified by the thermoelectric Figure of Merit ZT) to values greater than unity, entailing that their application to such tasks as the conversion of waste heat into electricity and refrigeration may now be practical (see, for instance, Reference [1]). In order to best direct research into which materials and nanostructures are most suited for which purposes, theoretical characterisations of the effects of nanostructuring on the electronic and lattice (phonon) properties of semi-conductor compounds must be developed. In what follows we discuss the detailed calculation of the lattice contribution to ZT, although we will devote some of our attention to approximate calculations of the electronic contributions needed to obtain the full Figure of Merit.

One of the most widely employed theoretical methods for calculating lattice thermal conductivity is the single-mode relaxation time approach to solving the phonon Boltzmann equation [2]. This approach has traditionally been applied to bulk materials using Debye's isotropic continuum approximation at harmonic as well as anharmonic levels, as detailed in Ref. [2]. Such an approach would be analytically tractable but would rely heavily on system-dependent parameters determined wholly by fitting to experimental results, since it would ignore many of the salient features of the system by, for instance having a continuum (rather than realistic) density of states. Its predictive usefulness in this case is therefore very limited. Recent advances in phonon studies aim at *ab initio* phonon conductivity computation, using accurate phonon dispersion curves and anharmonic force constants, and realistic Brillouin zone summation techniques (see, e.g. [3, 4]). For ultra-thin systems of the kind that we are interested in this entails the use of Density Functional Peturbation [DFPT] theory [5] in order to obtain the needed second- and third-order force-constants. However, a full descripton of the system at all temperatures of interest requires a treatment of third-order force constants in order to capture the behaviour of the most significant anharmonic contribution to the phonon scattering time. This is numerically challenging, somewhat opaque from a theoretical standpoint, and furthermore the values of the Grünneisen constants governing the strength of particular phonon exchanges have been shown to be particularly sensitive to truncation and other potential sources of error [6, 7]. Another problem associated with the *ab initio* approach is that the mode-average Grünneisen constant is also temperature dependent [2], whereas DFPT (being a Density Functional Theory technique) is carried out at $T = 0$. Ward and Broido's [4] calculations of phonon relaxation times for Si and Ge do show that changing the lattice constant of the system by the amount suggested by the theory of thermal expansion (hence 'effectively' increasing T) makes no significant difference to their results, and since most calculations (including our own) are carried out in the quasi-harmonic approximation [8], which excludes all effects of temperature change *other than* thermal expansion from consideration, this would seem to indicate that temperature is not a problem. We would caution against drawing overly optimistic conclusions from this success, however. Due to the complexity of the calculation and the number of force constants involved, it is possible that fortuitous cancellations of errors may be concealing the problem, or that thermal expansion might have negligible effects only for some systems. Our worry is that treating a fully *ab initio* approach as an oracular black box whose pronouncements are wholly trustworthy may lead us astray, and so

Electronic, Photonic, Plasmonic, Phononic and Magnetic Properties of Nanomaterials
AIP Conf. Proc. 1590, 95-104 (2014); doi: 10.1063/1.4870203

complementary methods are needed in order to further confirm its conclusions.

One such method would be a judicious combination of *ab inito* and semi-empirical approaches, as developed in our group over several years [9, 10, 11, 12]. In this approach we generate phonon eigensolutions for the system of interest from second-order force constants obtained by DFPT, and use them as input for analytically-derived expressions for the relevent contributions to the single-mode relaxation time. These expressions contain parameters which must be tuned through comparison with experiment in order to account for the relative strengths of relevant phonon scattering mechanisms. For alloys these include boundary, isotope, point-defect, alloy, carrier-phonon, and anharmonic scatterings. For superlattices there are two additional sources of phonon scattering: interface scattering and *mini-Umklapp* anharmonic interactions (due to the superlattice periodicity being larger than that of its constituent materials). For both alloys and superlattices sample-size, point-defects, and interface quality are dependent on the sample preperation method. The anharmonic interaction can be modelled so as to include an appropriate temperature dependence (and thus may also absorb effects external to the quasi-harmonic approximation into its behaviour, despite not formally including them). As a result of this partial dependence on experimental behaviour, this approach does lose some predictive power; however, it is possible to gain an understanding of the potential effects of nanostructuring on the system through (for example) altering the system from a superlattice to a periodic nanowire lattice while keeping the model parameters identical, and so make predictions as to what kind of structure is the most effective.

In what follows, we summarise previous calculations of ZT and the lattice contribution to the thermal conductivity for a SiGe alloy system and compare it with a superlattice system of identical size and doping in order to see the effects that nanostructuring has on the behaviour of the system.

METHOD

The figure of merit of a thermoelectric material is defined as

$$ZT = \frac{\sigma S^2 T}{\kappa_{\rm tot}}, \tag{1}$$

where σ is the electrical conductivity, S is the Seebeck constant, and $\kappa_{\rm el}$ and $\kappa_{\rm ph}$ respectively denote the carrier contribution and the lattice (phonon) contribution to the the thermal conductivity, and $\kappa_{\rm tot}$ is their sum.

The calculation of these quantities for the alloy case (whose results we review in this work) are determined by close comparison with the experimental data of Ref. [13]; since this determination is fairly involved, we refer those who are interested to Ref. [11], in which it is discussed in detail, and focus on the details of the calculation in the case of superlattices in what follows.

A component of the lattice thermal conductivity tensor of the superlattice system is calculated in the single-mode relaxation time approximation, and is given by [8, 2]:

$$\begin{aligned}\kappa_{\mu\nu} &= \frac{\hbar^2}{N_0 \Omega k_{\rm B} T^2} \\ &\times \sum_{\boldsymbol{q}s} \omega^2(\boldsymbol{q}s) c_{s,\mu}(\boldsymbol{q}) c_{s,\nu}(\boldsymbol{q}) \tau(\boldsymbol{q}s) \bar{n}_{\boldsymbol{q}s}(\bar{n}_{\boldsymbol{q}s}+1),\end{aligned} \tag{2}$$

where N_0 is the number of unit cells in the system, Ω their volume, T is the temperature, $\boldsymbol{q}$ and s label the wave vector and band number (i.e. polarization index) of a mode, $\omega(\boldsymbol{q}s)$ and $c_{s,\nu}(\boldsymbol{q})$ are the frequency and velocity components of a given mode (μ, ν label axes of the sample), and $\tau(\boldsymbol{q}s)$ is the relaxation time given by

$$\begin{aligned}\tau^{-1}(\boldsymbol{q}s) &= \tau^{-1}_{\rm LB}(\boldsymbol{q}s) + \tau^{-1}_{\rm MD}(\boldsymbol{q}s) + \tau^{-1}_{\rm el-ph}(\boldsymbol{q}s) \\ &+ \tau^{-1}_{\rm IMS}(\boldsymbol{q}s) + \tau^{-1}_{\rm AH}(\boldsymbol{q}s).\end{aligned} \tag{3}$$

Here, $\tau^{-1}_{\rm LB}(\boldsymbol{q}s)$, $\tau^{-1}_{\rm MD}(\boldsymbol{q}s)$, and $\tau^{-1}_{\rm el-ph}(\boldsymbol{q}s)$ are, respectively, the boundary, isotope and electron-phonon scattering rates and are calculated as in Ref. [11]. The Interface Mixing scattering (IMS) rate $\tau^{-1}_{\rm IMS}(\boldsymbol{q}s)$ arises from 'mass-smudging' (the formation of dislocations is neglected here, for the superlattice under consideration is well below the critical length for their formation [14]); for this and the anharmonic scattering rate $\tau^{-1}_{\rm AH}(\boldsymbol{q}s)$ we use the formulation from Ref. [12] (note that the formulation of the anharmonic term in [12] differs slightly from the version used in Ref. [11] to calculate the anharmonic scattering in the alloy).

It will be instructive to present the phonon relaxation rates $\tau^{-1}_{\rm IMS}(\boldsymbol{q}s)$ and $\tau^{-1}_{\rm AH}(\boldsymbol{q}s)$ for superlattice structures as derived in our previous work [12]. For a (m,n) superlattice with m layers of material A (mass m_A) and n layers of material B (mass m_B), the IMS rate can be expressed as

$$\begin{aligned}\tau^{-1}_{IMS}(\boldsymbol{q}s) &= \frac{\pi \Gamma_{\rm IMS}}{6N_0} \sum_{\boldsymbol{q}s} \omega(\boldsymbol{q}s)\omega(\boldsymbol{q}'s')\delta(\omega(\boldsymbol{q}s)-\omega(\boldsymbol{q}'s')) \\ &\times \frac{(\bar{n}_{\boldsymbol{q}'s'}+1)}{(\bar{n}_{\boldsymbol{q}s}+1)},\end{aligned} \tag{4}$$

where

$$\Gamma_{\rm IMS} = \mathscr{P}\left(\frac{\Delta M}{M}\right)^2 \left(\left[1-\frac{e_A e'_A}{e_B e'_B}\right]^2 + \left[1-\frac{e_B e'_B}{e_A e'_A}\right]^2\right), \tag{5}$$

and

$$\frac{e_B}{e_A} = \frac{\left[\frac{1}{M_0} - \Delta\left(\frac{1}{M}\right)\right]\cos(l_z q_z)}{\left[\left(\frac{1}{M_0}\right)^2 + \left\{\Delta\left(\frac{1}{M}\right)\right\}^2 \sin^2(l_z q_z)\right]^{1/2} - \Delta\left(\frac{1}{M}\right)}, \tag{6}$$

with $M = (mM_A + nM_B)$, $\Delta M = |M_A - M_B|$, $M_0 = (M_A^{-1} + M_B^{-1})/2$, $\Delta(1/M) = (M_A^{-1} - M_B^{-1})/2$, and l_z being the superlattice period in the z direction. The factor $\mathscr{P}$ determines the probability of interface mass mixing. The anharmonic scattering rate can be expressed as

$$\begin{aligned}\tau_{\rm AH}^{-1}(\boldsymbol{q}s) &= \frac{\pi\hbar\bar{\gamma}^2}{\rho N_0 \Omega \bar{c}^2} \sum_{\boldsymbol{q}'s',\boldsymbol{q}''s'',\boldsymbol{G}} \frac{\left(\mathscr{R}_{\boldsymbol{q}s,\boldsymbol{q}'s',\boldsymbol{q}''s''}\right)^2}{\omega(\boldsymbol{q}s)\omega(\boldsymbol{q}'s')\omega(\boldsymbol{q}''s'')} \mathscr{D}(\boldsymbol{q}, q', q'') \\ &\times \left[\frac{\bar{n}_{\boldsymbol{q}'s'}(\bar{n}_{\boldsymbol{q}''s''}+1)}{(\bar{n}_{\boldsymbol{q}s}+1)} \delta(\omega(\boldsymbol{q}s) + \omega(\boldsymbol{q}'s') - \omega(\boldsymbol{q}''s''))\delta_{\boldsymbol{q}+q',q''+\boldsymbol{G}}\right. \\ &\left. + \frac{1}{2}\frac{\bar{n}_{\boldsymbol{q}'s'}\bar{n}_{\boldsymbol{q}''s''}}{\bar{n}_{\boldsymbol{q}s}} \delta(\omega(\boldsymbol{q}s) - \omega(\boldsymbol{q}'s') - \omega(\boldsymbol{q}''s''))\delta_{\boldsymbol{q}+\boldsymbol{G},q'+q''}\right], \end{aligned} \tag{7}$$

wher $\bar{\gamma}$ is the mode-averaged Grüneissen constant, $\bar{c}$ is the long wavelength acoustic phonon speed, where ρ is the average mass density in the superlattice structure, and $\boldsymbol{G}$ is a reciprocal lattice vector. The term $\mathscr{R}$ can be expressed as

$$\begin{aligned}\mathscr{R} &= \left[\sqrt{\omega(i)\omega(j)}(\omega(i)+\omega(j))|\omega_\Gamma(k) - \omega(k)|\right. \\ &\left. + \text{similar terms with } i, j \text{ and} k \text{ interchanged}\right]/3!. \end{aligned} \tag{8}$$

The symbol $\mathscr{D}(\boldsymbol{q}, q', q'')$ represents a *dual mass term* and can be expressed as

$$\mathscr{D}(\boldsymbol{q}, \boldsymbol{q}', \boldsymbol{q}'') = \frac{1}{64}\left(\frac{\mathscr{A}_{AB}}{2\rho_A^{3/2}} + \frac{\mathscr{A}_{BA}}{2\rho_B^{3/2}}\right)^2 \tag{9}$$

where $\rho_{A(B)}$ is the density of material A(B) and

$$\begin{aligned}\mathscr{A}_{ij} &= 1 + \frac{\rho_i^{1/2}}{\rho_j^{1/2}}\left(\frac{e_j}{e_i} + \frac{e'_j}{e'_i} + \frac{e''_j}{e''_i}\right) \\ &+ \frac{\rho_i}{\rho_j}\left(\frac{e_j e'_j}{e_i e'_i} + \frac{e'_j e''_j}{e'_i e''_i} + \frac{e_j e''_j}{e_i e''_i}\right) + \frac{\rho_i^{3/2}}{\rho_j^{3/2}}\left(\frac{e_j e'_j e''_j}{e_i e'_i e''_i}\right), \end{aligned} \tag{10}$$

e_A and e_B being the vibrational eigenvectors in segments A and B, respectively.

The strength of the boundary scattering is controlled by the sample size L_B, that of the electron-phonon scattering by the acoustic deformation parameter E_D and the impurity concentration N_D, the isotope scattering by P, which scales it so as to include scattering from point impurities, and the anharmonic scattering by the mode-averaged Grüneissen constant $\bar{\gamma}$. The strength of the IMS scattering $\mathscr{P}$ must be modelled; our model is described in Ref. [12], but for our purposes it will suffice to say that the strength of IMS scattering is controlled by a pair of parameters controlling the probability of mass-mixing at the interface (B) and how quickly that probability falls away with distance from the interface (α). We choose values for two of these parameters based on our previous comparison with undoped experimental results [12]: that is, a scale factor of $P = 4.5$ for the point defect scattering rate, and $\bar{\gamma} = 0.45$ for temperatures below 150 K and $\bar{\gamma} = 0.45(1 + (T - 150)/150)^{0.56}$ above it. We take $N_D = 9.4 \times 10^{25}$ m^{-3}, the electron effective mass corresponding to the well (i.e. the Si mass; see below), $E_D = 10$ eV (slightly smaller than the value used in References [11] and [15]) and take $L_B = 0.2$ μm as per the alloy [11]. We parameterise $\mathscr{P}$ using $\alpha = 5.0$ and $B = 1.0$, which corresponds to a good quality interface [12]. Subject to momentum and energy conservation conditions, all allowed three-phonon Normal and Umklapp processes were included. For Umklapp scattering, we included reciprocal vectors with magnitude less than or equal to $G = 2\pi/a_0$, where a_0 is the cubic lattice constant.

The phonon eigensolutions required for the above calculation were generated using the DFPT package contained within QUANTUM ESPRESSO [16]. Energy minimisation was performed on a $10 \times 10 \times 2$ Monkhorst-Pack (MP) [17] grid using a kinetic energy cutoff of 15 Rd for the plane-wave basis, $a_0 = 5.54$ Å, and norm-conserving, local density approximation pseudopotentials [18]; the eigensolutions were generated from the dynamical matrices on a $16 \times 16 \times 12$ grid, which was found to give the best convergence in calculations on an undoped system [12].

We calculate the electronic contributions to ZT (that is S, σ and $\kappa_{\rm el}$) using the approximate nanostructure mixing formulae of Lin-Chung and Reineke [19]. In order to make use of these, we must first calculate the component contributions for the bulk and quantum well cases for both component species of the superlattice.

Using the charge conservation equation [20]

$$0 = N_D^{\rm ion} - n_0 + p_0, \tag{11}$$

where we assume complete ionisation so that the ionised donor contribution $N_D^{\rm ion} \approx N_D$, thermally exicted electron and hole concentrations are given by [20]

$$\begin{aligned} n_0 &= \frac{N_{\rm val}}{z_d a^{3-d}}\left(\frac{2k_{\rm B}Tm_e^{\rm dos}}{\hbar^2}\right)^{d/2} \mathscr{F}_{0.5d-1}(\beta_n), \\ p_0 &= \frac{N_{\rm val}}{z_d a^{3-d}}\left(\frac{2k_{\rm B}Tm_p^{\rm dos}}{\hbar^2}\right)^{d/2} \mathscr{F}_{0.5d-1}(\beta_p), \end{aligned} \tag{12}$$

where $d = 2(3)$ for two(three)-dimensional system, $m_{p(n)}^{\rm dos}$ is the hole(electron) density of states mass, a is the well width, E_c and E_v are the conduction and valence band edges,

$$z_2 = 2\pi, \quad z_3 = 2\pi^2,$$
$$\beta_n = \eta_R - ((E_c + (3-d)E_1^e)/k_{\rm B}T),$$

$$\beta_p = (E_v - (3-d)E_1^p)/k_B T) - \eta_R,$$
$$E_1^{e(p)} = \hbar^2\pi^2/2a^2 m^{\rm dos}_{e(p)},$$

$\eta_R = E_F/k_B T$ is the reduced Fermi energy, and $\mathscr{F}_n(y)$ is the Fermi integral

$$\mathscr{F}_n(y) = \int_0^\infty \frac{x^n}{e^{x-y}+1}.$$

We can determine the reduced Fermi energy for systems of a given temperature and dimensionality d through use of the Van-Wjingaarden-Decker-Brent method [21]. From this, we may calculate the electronic components using the subsequent expressions.

When calculating σ we assume that the dominant scattering process is acoustic phonon scattering. In that case, from the expressions in [22] (for the the bulk case) and [23] (for the 2D case) we can show that the exponent of the energy dependence of the scattering s is equal to -0.5 in the bulk case and 0 for quantum wells, and that (via Ref. [24]),

$$\begin{aligned}\sigma^{\rm 3D}_{n,p} &= \frac{2N_{\rm val}e^2\hbar\rho c_L^2}{3\pi E_D^2 m_c^*}\mathscr{F}_0(x),\\ \sigma^{\rm 2D}_{n,p} &= \frac{4N_{\rm val}e^2\hbar\rho c_L^2}{3\pi E_D^2 m_c^*}\mathscr{F}_0(x).\end{aligned} \quad (13)$$

Here, $N_{\rm val}$ is the number of valleys, c_L is the speed of the longitudinal phonon mode in the long-wavelength limit, E_D is the acoustic deformation potential, m_c^* is the conduction mass and ρ is the density of the material. $x \equiv \beta_n$ for electrons and $x \equiv \beta_p$ for holes. The other electronic contributions are given by [24, 25]

$$\begin{aligned}S &= \mp\frac{k_B}{e}\left(\mathscr{M}(x) - x\right),\\ \mathscr{M}(x) &= \frac{(s+0.5d+1)\mathscr{F}_{s+0.5d}(x)}{(s+0.5d)\mathscr{F}_{s+0.5d-1}(x)},\end{aligned} \quad (14)$$

where electrons use the negative sign and holes the positive, and

$$\begin{aligned}\kappa_{\rm el} &= \frac{k_B^2}{e^2}\Bigg\{\mathscr{L}(\beta_n)\sigma_n T + \mathscr{L}(\beta_p)\sigma_p T\\ &+ \frac{\sigma_n\sigma_p T}{\sigma_n+\sigma_p}\left[\beta - \alpha + \mathscr{M}(\beta_n) + \mathscr{M}(\beta_p)\right]^2\Bigg\},\\ \mathscr{L}(y) &= \frac{1}{(s+0.5d)^2\mathscr{F}_{s+0.5d-1}(y)^2}\\ &\times\Bigg[(s+0.5d+2)(s+0.5d)\mathscr{F}_{s+0.5d+1}(y)\mathscr{F}_{s+0.5d-1}(y)\\ &-(s+0.5d+1)^2\mathscr{F}_{s+0.5d}(y)\Bigg].\end{aligned} \quad (15)$$

To get the total σ and total S we simply sum hole and electron contributions as follows:

$$\begin{aligned}\sigma_{\rm tot} &= \sigma_n + \sigma_p,\\ S_{\rm tot} &= \frac{\sigma_n S_n + \sigma_p S_p}{\sigma_{\rm tot}}.\end{aligned} \quad (16)$$

For Si, we chose $m^{\rm dos}_{e(p)} = 0.33(0.55)m_e$, $m_c^* = 0.26(0.24)m_e$, $N_{\rm val} = 6(1)$ for electrons (holes) (derived from the values in Reference [20]), $E_v = E_c - 1.2$ eV [20], and $\rho = 2329$ kg/m^3 [26]. For Ge, we chose $m^{\rm dos}_{e(p)} = 0.22(0.29)m_e$, $m_c^* = 0.12(0.08)m_e$, $N_{\rm val} = 4(1)$ for electrons (holes) (also derived from the values in Reference [20]), $E_v = E_c - 0.72$ eV [20], and $\rho = 5323$ kg/m^3 [26]. $E_c = 0.0$eV, $a_0 = 11.08$ Åand $E_D = 10$eV in all cases, as per the discussion of the electron-phonon term in the lattice conductivity calculation above. For reasons of simplicity, we are using the bulk values of the electron and hole parameters for the constituents.

The mixing formulae [19] contain the following labels. The subscript 'SL' indicates the mixed value for the superlattice, 'w' the value for the well component (in this case Si) and 'b' the barrier component (in this case Ge). The superscript 'bk' indicates a bulk value, 'qw' a quantum well value, and 'in' and 'cross' that a mixed value corresponds to the in-plane or cross-plane value respectively. We define $\gamma = \kappa_{\rm tot} + \sigma S^2 T$ where the sub- and super-scripts are assumed to match (note that κ in the following formulae corresponds to $\kappa_{\rm tot}$).

The in-plane formulae are [19]:

$$\begin{aligned}\sigma^{\rm in}_{\rm SL} &= \frac{a_{\rm w}\sigma^{\rm qw}_w + a_{\rm b}\sigma^{\rm bk}_b}{a_{\rm w}+a_{\rm b}},\\ \gamma^{\rm in}_{\rm SL} &= \frac{a_{\rm w}\gamma^{\rm qw}_w + a_{\rm b}\gamma^{\rm bk}_b}{a_{\rm w}+a_{\rm b}},\\ S^{\rm in}_{\rm SL} &= \frac{a_{\rm w}\sigma^{\rm qw}_w S^{\rm qw}_{\rm w} + a_{\rm b}\sigma^{\rm bk}_b S^{\rm qw}_{\rm b}}{a_{\rm w}\sigma^{\rm qw}_w + a_{\rm b}\sigma^{\rm bk}_b}.\end{aligned} \quad (17)$$

The cross-plane formulae are [19]:

$$\begin{aligned}\sigma^{\rm cross}_{\rm SL} &= \frac{\sigma^{\rm bk}_{\rm w}\kappa^{\rm bk}_{\rm w}}{a_{\rm w}}AW,\\ \gamma^{\rm cross}_{\rm SL} &= \frac{\sigma^{\rm bk}_{\rm w}\kappa^{\rm bk}_{\rm w}}{a_{\rm w}}\left(\gamma^{\rm bk}_{\rm w} + q\gamma^{\rm bk}_{\rm b}\right)W,\\ S^{\rm cross}_{\rm SL} &= \frac{B}{a_{\rm w}\sigma^{\rm bk}_{\rm w} + a_{\rm b}\sigma^{\rm bk}_{\rm b}},\end{aligned} \quad (18)$$

where

$$\begin{aligned}A &= \sigma^{\rm bk}_{\rm w} + q\sigma^{\rm bk}_{\rm b}, \qquad W \equiv \frac{a_{\rm w}+a_{\rm b}}{A\left(\sigma^{\rm bk}_{\rm w} + q\sigma^{\rm bk}_{\rm b}\right) - TB^2},\\ B &= \sigma^{\rm bk}_{\rm w}S^{\rm bk}_{\rm w} + q\sigma^{\rm bk}_{\rm b}S^{\rm bk}_{\rm b}, \qquad q = \frac{a_{\rm b}\sigma^{\rm bk}_{\rm w}\kappa^{\rm bk}_{\rm w}}{a_{\rm w}\sigma^{\rm bk}_{\rm b}\kappa^{\rm bk}_{\rm b}}.\end{aligned} \quad (19)$$

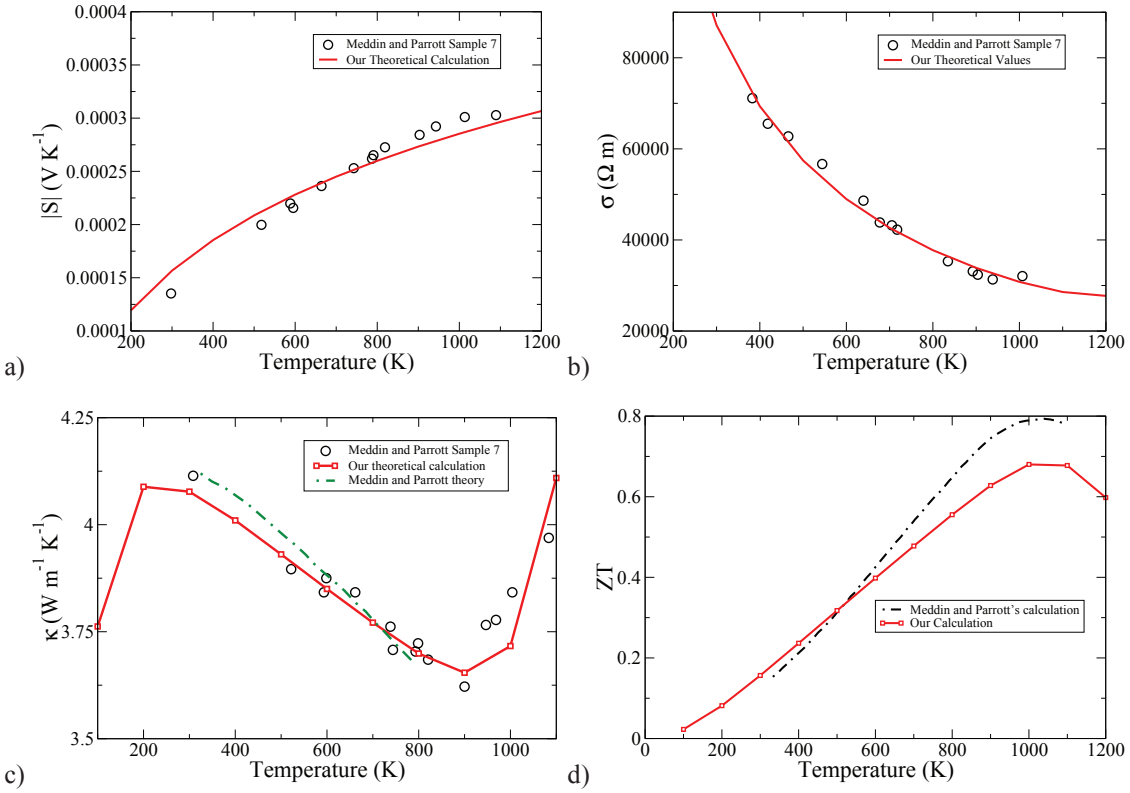

FIGURE 1. Alloy results fitted semi-empirically to experimental data from [13] . a) shows the behavior of the Seebeck constant with temperature, b) the conductivity, c) the total thermal conductivity and d) the Figure of Merit ZT. (Figures are taken from [11], and data from [13] is used with permission of IOP publishing Ltd.)

RESULTS

SiGe Alloy

Figure 1 displays the results [11] of our calculation of $\kappa_{\rm ph}$ (included within the total thermal conductivity κ in Figure 1 c)) and our modelling of the electronic contributions alongside the experimental results from Ref. [13] for a $Si_{0.754}Ge_{0.246}$ alloy doped with a concentration of 9.4×10^{25} m^{-3} of P donor atoms. Firstly, we can see that we have a good match with experimental results for all components, and a somewhat better match for κ than the theory in Ref. [13]. In general, we see that the system is generally extrinsic in nature; the only noticible effect of thermally excited holes can be seen in the bi-polar contribution to κ in Fig. 1 c) that causes it to increase for $T > 900$ K. The thermal conductivity is relatively 'flat' over the temperature range considered, generally remaining within 10% of 4 W m^{-1} K^{-1}, probably due to the sintering of the system, which results in the formation of small crystallite structures that push the effective size of the system down to $L_B \approx 0.2$ μm and so suppress the low-temperature peak. Our overall ZT results are somewhat similar to those in Ref. [13], although our peak value ($ZT \approx 0.68$ at 1000 K) is somewhat (≈ 16 %) smaller than theirs.

SiGe superlattices

We present results for the Si(4)Ge(4)[001] superlattice, with each unit cell along the [001] growth direction containing 4 bilayers of Si and 4 bilayers of Ge. When presenting the $\kappa_{\rm ph} = \{\kappa_{\mu\mu}\}$ results, we have taken our x and y axes to be the [110] and [110] axes respectively, and z to be the [001] growth direction (i.e. the cross-planar direction). Figure 2 shows the behaviour of the various components of the lattice thermal conductivity. We should note that while κ_{xx} and κ_{yy} are quantitatively and qualitatively very similar, they are not identical (we have discussed this discrepancy in [27]), but they are much larger than κ_{zz} (about 6 times larger at 300 K).

It has been observed [20] that theoretical treatments of the electrical conductivity and related quantities of the kind that we have performed here rarely produce results exactly matching those of experiment since they exclude the effects of inelastic scattering processes. It is therefore often necessary to rescale fits by an *ad hoc* factor

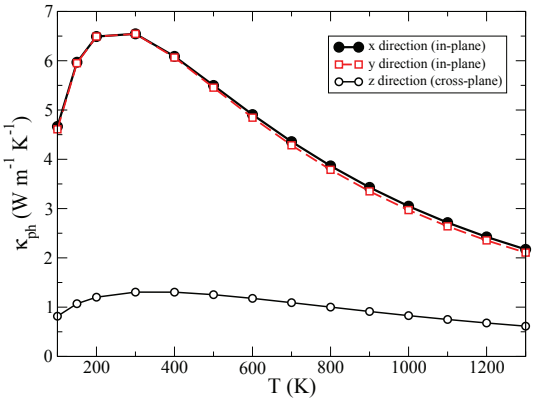

FIGURE 2. Thermal conductivity results for the lattice contributions to the thermal conductivity in in-planar and cross-planar directions.

[20, 28] that absorbs these effects, and this proved necessary in the fitting of the electrical conductivity in our alloy study [11]. A problem presents itself: if we wish to make a fair comparison between our two systems, we should also rescale the superlattice conductivities by a similar amount. However, we have no experimental results on which to base such a rescaling. In the absence of such, we therefore rescale our conductivity results by the factor $0.0013T^{0.4}$ that we used for the alloy, which then alters all quantities dependent on them [11]. This can provide us with a conservative estimate of the effects of superlattice structuring; in fact it is extremely unlikely that this factor would be identical in such a system and (unlike in our calculations) it is unlikely that it would be identical for both hole and electron contributions. The results of following this rescaling are displayed in Figure 3. σ is of a similar order of magnitude to the alloy electrical conductivity, and the in-plane and cross-plane curves intersect in the vicinity of 400-500 K. The behaviour of S is fairly similar, and the overall power factor σS^2 is an order of magnitude *less* than that of the alloy. κ_{el} is smaller than unity and so the behaviour of κ_{tot} is dominated by the behaviour of the lattice contributions (as can be seen from a comparison of Figure 2 b) with 3 d)), and again there is no significant bipolar contribution (though this may be an artefact of our using identical rescaling factors for both holes and electrons). We can see a (small) improvement in ZT relative to the alloy in the cross-plane direction but the in-plane direction is much less efficient. This is because the cross-planar thermal conductivity is consistently less than the alloy thermal conductivity while the in-planar thermal conductivity is either greater (low temperatures) or only slightly smaller (high temperatures); between this and the small power factors this entails that ZT for the in-plane case is much smaller than for the alloy, and the cross-planar case is at best only slightly better.

However, this is based on pessimistic assumptions. As we have said, there is no reason to believe that any rescaling due to the effects of inelastic collisions will be as extreme as we have assumed. It is therefore reasonable to perform calculations in the absence of such a factor in order to estimate an upper-bound to enhancements. Figure 4 displays the in-plane and cross-plane values of the electrical conductivity, the Seebeck constant, and the total thermal conductivity calculated from the bulk and quantum well values using equations (17) to (19) in the absence of rescaling. Similarly to the rescaled case, the values of the in-plane and cross-plane electrical conductivity are roughly comparable, but are not identical: at low temperatures the cross-plane results are noticably larger than the in-plane results but at high temperatures they are slightly smaller, though the curves cross in the range $300 - 400$ K in this case rather than in the range $400 - 500$ K. The Seebeck constant is identical to that of the rescaled case, and its directional dependence more obvious than for σ; we can see that while the cross-planar result is slightly larger at 100 K, the values intersect at 200 K, and thereafter the in-plane values are larger, with the two sets of results diverging further as T increases. For κ_{tot}, the bulk results show a similar behaviour with temperature, with the Si results being (very roughly) half those of Ge. The quantum well results for Si are well above those for Ge, and show a sharp increase towards 100 K, while levelling off at higher temperatures. The bipolar contribution is too small to be seen, a sign that the system is well with in the extrinsic regime for the entire temperature range. The total values following mixing using the LR formulae show that the in-plane thermal conductivity is between 2-3 times that of the cross-plane conductivity, and that unlike the rescaled case the effects of the electrical contributions dominate over those of the lattice contributions, since the magnitude of the curves most is closer to that of the electronic contributions than the phonon contributions .

The overall Figure of Merit and a comparison of power

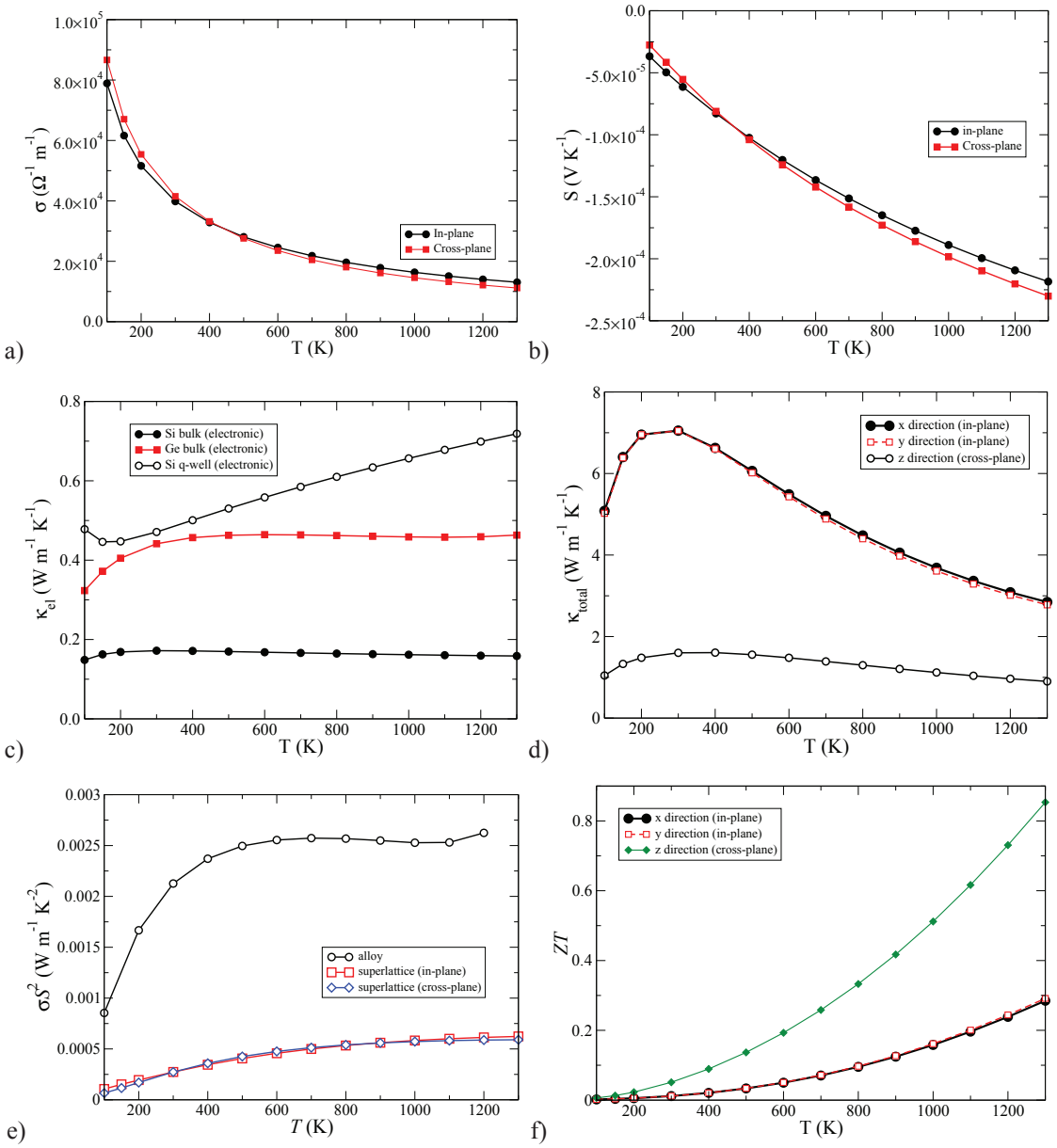

FIGURE 3. Results for the (4,4) superlattice system with rescaled conductivity. a) shows the conductivity, b) the Seebeck constant, c) the electronic contributions to the thermal conductivity prior to mixing, d) the total thermal conductivity following mixing, e) the in-plane and the cross-plane power factors compared with the power factor calculated from the results of [11], and f) the overall *ZT* in each direction.

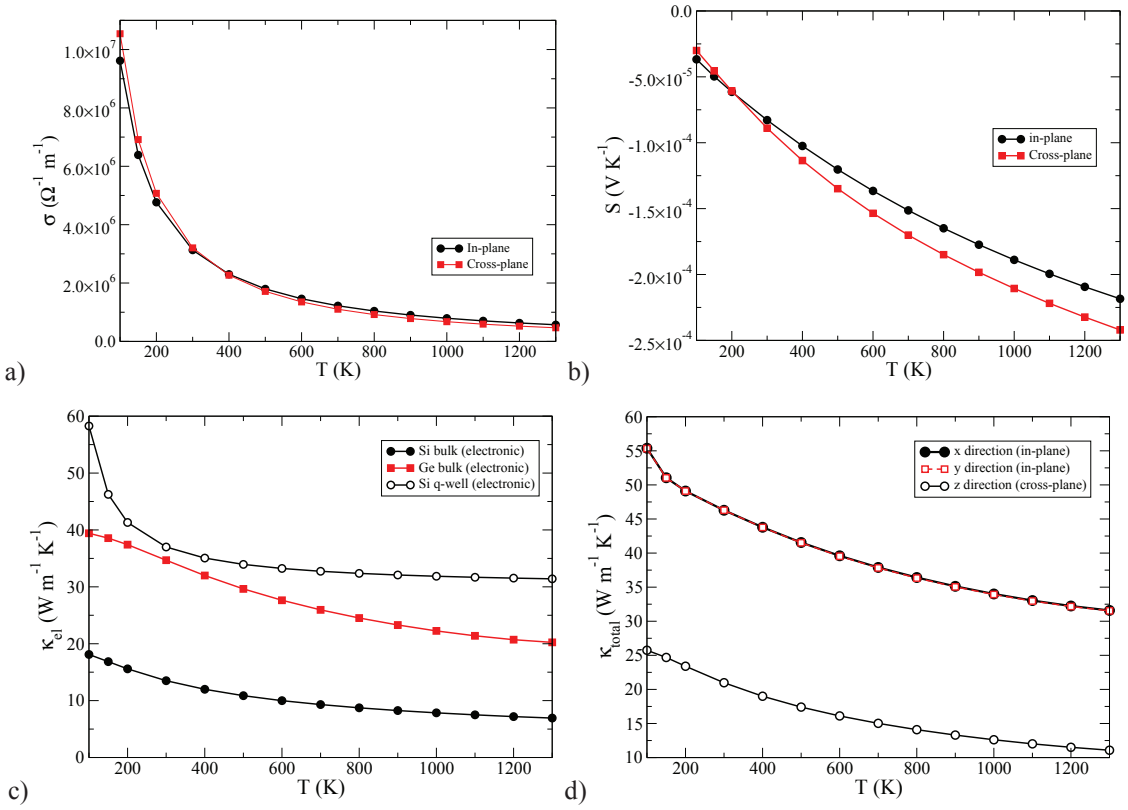

FIGURE 4. The a) conductivity, b) Seebeck constants, c) electronic contribution to thermal conductivity and d) total thermal conductivity in the in-plane and cross-plane directions for the (4,4) superlattice without rescaling.

factors is shown in Figure 5. Here we can see that the power factors for the superlattice for both in-plane and cross-plane directions are an order of magnitude or so greater than that of the alloy. For most of the temperature range considered ($\approx$ 1300 K $T >\approx$ 200 K) , the cross-plane values are greater than those of the in-plane case, most likely because for this range the absolute value of the cross-plane S is large enough relative to the in-plane S to compensate for any similarity in σ. This partly explains the most striking aspect of these results, which is that the ZT calculated is well above unity for the cross-planar direction for $T >\approx$ 550 K (indeed the increase in efficiency relative to the alloy results in Fig. 1 is rather large), while the in-plane results remain below unity for $<\approx$ 1200 K. However, the difference in ZT is greatest at 1300 K, where the power factors are almost identical. This can be explained with reference to the thermal conductivity. Since the in-plane κ_{tot} is ≈ 3 times larger than κ_{tot} in the cross-plane direction, we would expect ZT for the in-plane direction to be roughly three times smaller than in the cross-planar direction, and this is in fact what we see. That ZT in the cross-planar case is larger than in the in-planar case *and* greater than the bulk or alloy values is a significant difference from Lin-Chung and Reinecker's original results [19]; we ascribe this to our use of a more accurate calculation of the phonon thermal conductivity than used in that work, where bulk values of the phonon conductivities were used.

What can we conclude from this? Firstly, that at worst the rescaled case is most likely a lower bound. It is unlikely that the rescaling factor is correct for the superlattice case, and a more careful analysis of the processes involved or a set of good quality experimental results might well show that it is too small. However, even were we to allow that it would be fairly similar, further improvements in ZT are still be possible, since the total thermal conductivity is now dominated by the lattice contribution. Two possible routes for improvement now suggest themselves: reducing L_B, since this can have a strong effect on κ_{ph} – especially at low temperatures [29], and worsening the interface quality. The former is likely limited by the minumum size to which a superlattice can be reduced (that is, the size of one period) and by fabrication constraints, but that last could have a noticable effect, particularly as the IMS model parameters which we are using correspond to a fairly clean interface [12]. One last possibility is that the presence of so many dopant ions in the system will also lead to an increase in the number of

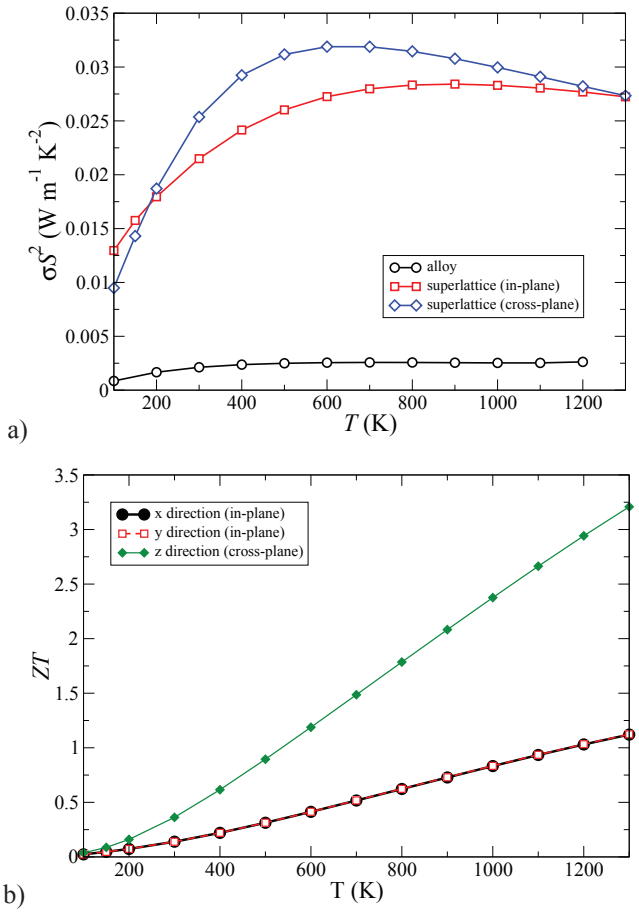

FIGURE 5. a) Comparison of power factor for alloy (calculated from results in [11] with power factor for superlattice, b) Figure of Merit in all directions for the (4,4) superlattice without scaling.

point impurities in the system, which in turn would be accounted for by an increase in the parameter P used in the calculation of κ_{ph}, which would cause κ_{ph} to decrease and hence increase ZT. Our calculations do not account for this possibility, as we know of no way of modelling a relation between N_D and P, and so perhaps overestimate the lattice contribution to the thermal conductivity.

Secondly, if – as seems entirely possible – the true behaviour of the superlattice system is somewhere between the rescaled and unrescaled extremes, we can predict that superlattice structuring leads to a noticable improvement in the thermoelectric efficiency that can, in principle, be quite large. The true extent to which this is so, however, awaits detailed calculations of the electronic contributions to the Figure of Merit that are beyond the scope of the present work.

Lastly, a few more general caveats are in order: as this system is very thin, we would expect that the effects of carrier tunnelling would be significant in a real system where the potential barrier of the quantum well is finite [19]. This means that we would expect our prediction of ZT to be an overestimate. Furthermore, our calculation in the cross-planar direction ignores the full effects of confinement on the electron band structure; however, the potential improvement is so large that even if our calculations overestimate its extent, given some of the considerations in the preceeding discussion, it seems plausible that some significant increase in ZT could still be observed.

CONCLUSIONS

We have reviewed the results of our previous calculation of ZT for a n-doped SiGe alloy and presented the results of new calculations for the ZT of a (4,4) SiGe superlattice, with an emphasis on the effects of the sample size L_B on the thermal conductivity and Figure of Merit. We obtain the thermal conductivity through a combination of DFPT and a semi-empirical method, and use appropriate modelling techniques to estimate the electronic contributions.

We conclude that in principle, superlattice structuring can lead to a great increase in ZT in the cross-planar direction, and a much smaller increase for the in-plane directions. ZT is greater than unity in the cross-planar directions for a wide temperature range, but only for a small range in the in-plane direction. If an ad-hoc factor determining the effects of inelastic processes is included, the improvements appear to become marginal at best; however, in that case it is possible that the use of superlattices with poor interface quality (and hence lower lattice thermal conductivities) could still result in improvements to the Figure of Merit. Due to the simplifications involved, however, the latter case most likely represents a worst-case scenario – improvements to ZT arising from superlattice structuring may still be rather more noticable than it predicts, but it demonstrates that more analysis is needed in order to properly understand the behaviour of the electronic contributions of ZT in addition to the lattice contributions.

We would therefore contend that the improvements in ZT due to the effects of nanostructuring on the lattice thermal conductivity should persist in more detailed calculations, and should also be observable in experiment.

REFERENCES

1. G. Chen, M. S. Dresselhaus, G. Dresselhaus, J.-P. Fleurial and T. Caillat, Int. Metall. Rev. **48**, 45 (2003).
2. G. P. Srivastava, *The Physics of Phonons* (Adam Hilger, Bristol, 1990).
3. D. A. Broido, M. Malomy, G. Birner, N. Mingo, and D. A. Stewart, Appl. Phys. Lett. **91**, 231922 (2007).
4. A. Ward and D. A. Broido, Phys. Rev. B **81**, 085205 (2010).
5. S. Baroni, S. de Gironcoli, A. Dal Corso, and P. Giannozzi, Rev. Mod. Phys. **73**, 515 (2001).
6. M. Lopuszyński and J. A. Majewski, Phys. Rev. B **76**, 045202 (2007).
7. K. Esfarjani, G. Chen, and H. T. Stokes, Phys. Rev. B **84**, 085204 (2011).
8. J. M. Ziman, *Electrons and Phonons* (Oxford University Press, Oxford, New York, 1967).
9. S. P. Hepplestone and G. P. Srivastava, Phys. Rev. B **82**, 144303 (2010).
10. S. P. Hepplestone and G. P. Srivastava, Phys. Rev. B **84**, 115326 (2011).
11. I. O. Thomas and G. P. Srivastava, Phys. Rev. B **86** 045205 (2012).
12. I. O. Thomas and G. P. Srivastava, accepted for publication by Physicial Review B.
13. H. R. Meddins and J. E. Parrott, J. Phys. C: Solid State Phys. **9**, 1263 (1976).
14. S.-M. Lee, D. A. Cahill, and R. Venkatasubramanian, Appl. Phys. Lett. **70**, 2957 (1997).
15. A. J. Minnich, H. Lee, X. W. Wang, G. Joshi, M. S. Dresselhaus, Z. F. Ren,2 G. Chen,and D. Vashaee, Phys. Rev. B **80**, 155327 (1990).
16. P. Gianozzi *et al.*, J. Phys. Cond. Mat. **21**, 395502 (2009); code available from [http://www.quantum-espresso.org].
17. H. J. Monkhorst and J. D. Pack, Phys. Rev. B 13, 5188 (1976).
18. The pseudopotentials Si.pzvbc. UPF and Ge.pz-bhs.UPF, available from [http://www.quantum-espresso.org].
19. P. J. Lin-Chung and T. L. Reinecke, Phys. Rev. B **51**, 13244 (1995).
20. J. P. McKelvey, *Solid State and Semiconductor Physics* (International Edition) (Harper and Row, New York, Evanston, London, and John Weatherhill Inc., Tokyo, 1966).
21. W. H. Press, B. P. Flanney, S. A. Teukolsky, and W. T. Vetterling, *Numerical Recipies: The Art of Scientific Computing* (Cambridge University Press, Cambridge, 1986), pp. 352-355.
22. B. R. Nag, *Theory of Electrical Transport in Semiconductors* (Pergamon, Oxford, 1972).
23. B. K. Ridley, J. Phys. C: Solid State Phys.**15**, 5899 (1982).
24. P. Pichanusakorn and P. Bandaru, Mat. Sci. and Eng. R **67**, 19 (2010).
25. J. R. Drabble and H. J. Goldsmit, *Thermal Conduction in Semiconductors* (Pergamon, Oxford, 1961).
26. *Landolt-Börnstein Numerical Data and Functional Relationships in Science and Technology: Group III*, edited by O. Madelung, M. Schulz, and H.Weiss (Springer-Verlag, Berlin, Heidelberg, New York, 1982), Vol. 17a.
27. I. O. Thomas and G. P. Srivastava, Phys. Rev. **87**, 085410 (2013).
28. O.C. Yelgel and G. P. Srivastava, Phys. Rev. B **85**, 125207 (2012).
29. M. N. Luckyanova *et al.*, Science **338**, 936 (2012).